Supplementary Information for:

Endothermic physiology of extinct megatooth sharks

Michael L. Griffiths[a1]†, Robert A. Eagle[b1]†, Sora L. Kim[c1]†, Randon J. Flores[b], Martin A. Becker[a], Harry M. Maisch IV[d], Robin B. Trayler[c], Rachel L. Chan[c], Jeremy McCormack[e], Alliya A. Akhtar[a,f], Aradhna K. Tripati[b], Kenshu Shimada[g-i1]

Affiliations:
[a]Department of Environmental Science, William Paterson University of New Jersey, 300 Pompton Road, Wayne, New Jersey 07470, USA.
[b]Department of Atmospheric and Oceanic Sciences, Department of Earth, Planetary, and Space Sciences, Institute of the Environment and Sustainability, Center for Diverse Leadership in Science, University of California - Los Angeles, Los Angeles CA 90095 USA.
[c]Department of Life and Environmental Sciences, University of California - Merced, Merced, California 95343, USA.
[d]Department of Marine and Earth Sciences, Florida Gulf Coast University, Fort Myers, FL 33965, USA.
[e]Institute of Geosciences, Goethe University Frankfurt, 60438 Frankfurt am Main, Germany.
[f]Department of Geosciences, Princeton University, Princeton, NJ 08544.
[g]Department of Environmental Science and Studies, DePaul University, 1110 West Belden Avenue, Chicago, Illinois 60614, USA.
[h]Department of Biological Sciences, DePaul University, 2325 North Clifton Avenue, Chicago, Illinois 60614, USA.
[i]Sternberg Museum of Natural History, Fort Hays State University, Hays, Kansas 67601, USA.

[1]To whom correspondence may be addressed. Email: griffithsm@wpunj.edu; robeagle@g.ucla.edu; skim380@ucmerced.edu; kshimada@depaul.edu

†These authors contributed equally to this work.

This PDF file contains:

1. Supplementary Results

1.1 $\delta^{18}O_p$ data compared to published analyses

Following previous $\delta^{18}O_p$ studies focused on sharks and Mesozoic marine reptiles (1, 2), we adopted the approach of calculating the difference in $\delta^{18}O_p$ values between coexisting *Otodus* taxa and ectothermic taxa across all sites, and then plotted this difference as a function of $\delta^{18}O_p$ values of ectothermic taxa (Fig. S1). Using the methodology of Bernard *et al*. (2), calculated regression lines that have a more negative slope (i.e., those closer to -1) imply that body temperatures for the species in question are to some extent independent of ambient seawater temperatures, thereby ruling out ectothermic physiology. In addition, we plotted this relationship alongside previously published $\delta^{18}O_p$ values from teeth of Cretaceous-Miocene megatooth sharks (ref. 1 and references therein; Fig. S1A). Calculated regression lines with and without our data show no significant difference in slopes (P_{slope} = 0.8197), and collectively exhibit a significant deviation from a slope of 0 (P_{slope} = 0.001) that would imply the taxa were ectothermic. Furthermore, the slope of a regression through all the marine reptile data from Bernard *et al. (2)* and all *Otodus* sp. data were not significantly different from each other (P = 0.4544) (Fig. S1B).

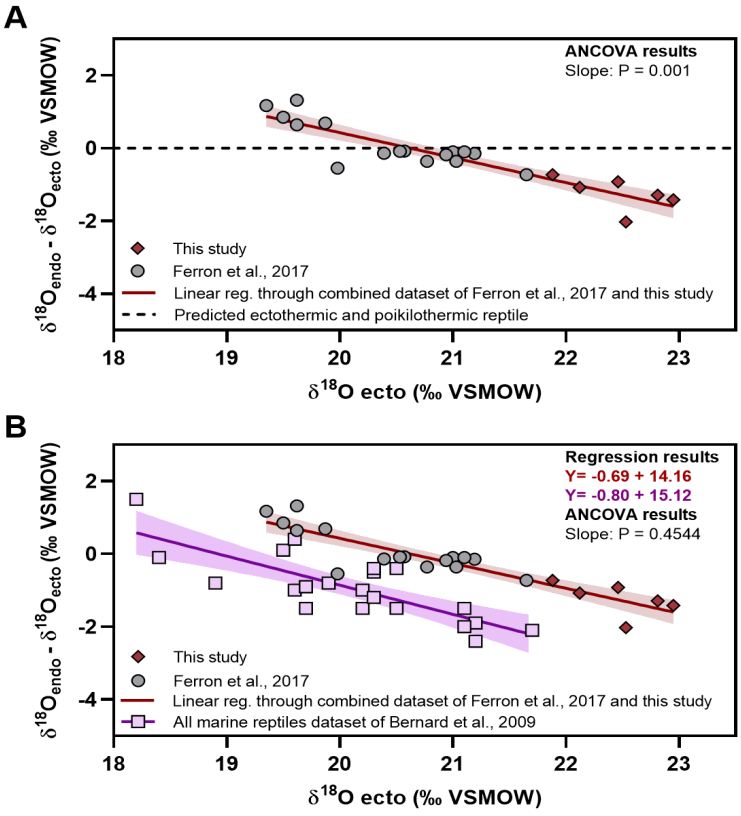

Fig S1. (A) Data generated in this study added to that of Ferron *et al.*(1). **(B)** Compared to the marine reptile data of Bernard *et al*. (2).

1.2 Modern elasmobranch bioapatite Δ_{47}-temperature calibration compared to published calibrations

To compare the results of our apatite calibration with recently published calibration datasets in addition to the Anderson *et al*. (3) calibration included in the main text, we conducted ANCOVA tests on our bioapatite dataset and the datasets of Loffler *et al*. (4), Petersen *et al*. (5), and Defliese and Tripati (6) (Fig. S2). These comparisons were calculated using the Prism software package.

The calibration dataset of Loffler *et al*. (4) consists of both synthetic carbonate-substituted apatite and natural bioapatite samples including teeth from terrestrial vertebrates and sharks. The calibration covers a formation temperature range of ~1 ºC to 80 ºC and is represented by eight samples and 122 Δ_{47} measurements. This study was carried out with a 110 ºC acid digestion temperature for the purpose of expediting reaction times to ensure complete sample digestion and was not reported with an acid fraction factor to correct back to 25 ºC. To compare this dataset to ours, we first corrected the reported Δ_{47} values presented in Table S1 to 25 ºC using the acid fractionation factor for calcite at 110 ºC from Defliese *et al*. (6). We then projected the resulting values into the I-CDES reference frame following the transfer function method outlined in Bernasconi *et al*. (7) for translating Δ_{47} values reported in CDES to I-CDES. The ANCOVA test between our dataset and these recalculated data yielded P values of 0.3763 and 0.1251 for the slopes and intercepts of the regression lines, respectively. The absence of a statistically significant difference in slope and intercept between the calibration produced in this study and that of Loffler *et al*. (4) demonstrates that, while 110ºC acid digestion temperatures for bioapatite may be of benefit for achieving complete digestion of the sample, the data presented here confirms previous observations that 90 ºC acid digestion temperatures and the use of a "Passey Style" semi-automatic sample reaction and CO_2 gas purification system can produce robust Δ_{47} data from apatite bound carbonates (8-10) which show Δ_{47}-temperature relationships indistinguishable from calcite (3, 11).

The Petersen *et al*. (5) calibration combined data from 14 studies including eight synthetic datasets and six organic or natural datasets comprising a total of 262 Δ_{47} measurements, all of which were recalculated using the parameters defined by Brand *et al*. (12). When compared to the calibration dataset of this study, an ANCOVA test yields a P value of 0.7710 for the slopes and 0.6207 for the intercepts. Once again, these results indicate that there is no statistical difference in the Δ_{47} temperature relationship between our bioapatite-based dataset and a large dataset derived from a variety of carbonate material types.

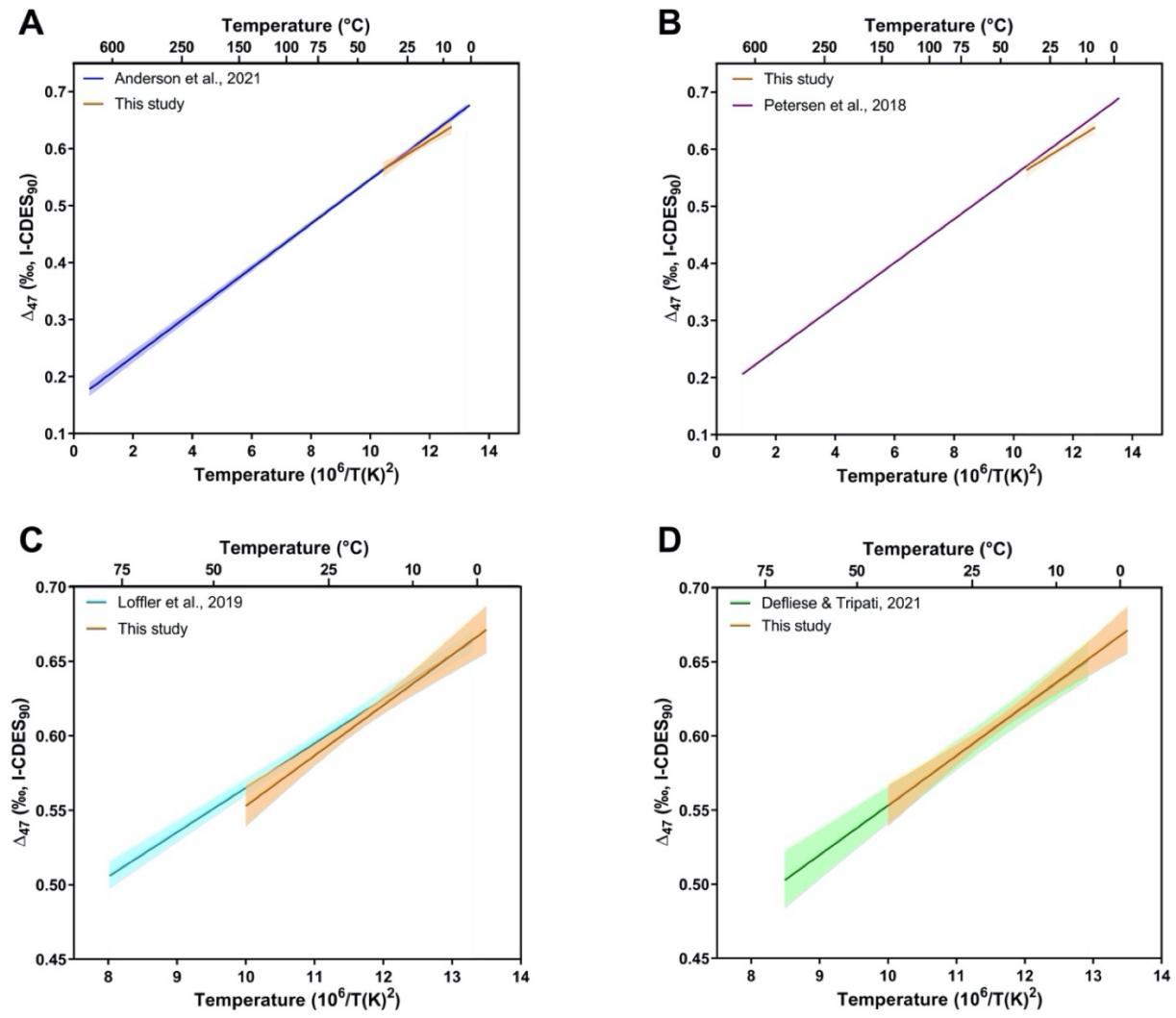

Fig. S2. Comparison of various published Δ_{47}-temperature calibration lines. Shaded regions surrounding regression lines indicate 95% confidence intervals. The linear regression of data from this study (orange line) is compared with published calibration lines from **(A)** Anderson *et al.* (3) (blue line), **(B)** Petersen *et al*. (5) (pink line), **(C)** Loffler *et al*. (4) converted onto the I-CDES reference frame with an acid digestion correction determined on calcite (turquoise line), and **(D)** Defliese and Tripati (6) (green line). The comparison between this study and Anderson *et al*. (3) is displayed in the main text but shown here to present the calibration line over the full temperature range of samples comprising the calibration. ANCOVA tests reveal no statistical difference in slopes or intercepts of our apatite calibration to these carbonate calibrations.

The Defliese and Tripati (6) dataset consists of 22 Δ_{47} measurements performed on five laboratory precipitated calcite samples analyzed in the Tripati laboratory at the University of California, Los Angeles. This study reported Δ_{47} values in a variety of standardization schemes, but for the purposes of comparison to the data in our study, we selected those Δ_{47} values from Defliese and Tripati (6) that were corrected using a combination of gas and carbonate standards in the non-linearity correction and carbonate standards used only in the empirical transfer function were obtained from supplemental information Table S1. These values were projected into the I-CDES reference frame using the ETH-1, 2, and 3 values of Bernasconi *et al*. (7) calculated in the Easotope software package (13). The results of an ANCOVA test between this dataset and our bioapatite dataset yield a P value of 0.9191 for the slope and 0.8480 for the intercept. This result confirms consistency between analyses performed in the same laboratory over different time periods following the same analytical procedure.

2. Supplementary Methods

2.1 Description of specimens

Specimens from Onslow Bay, North Carolina, and Summerville, South Carolina, USA

The continental shelf of Onslow Bay contains Cenozoic marine sediments that overlie high-relief crystalline basement rocks of the Carolina Platform and the mid-Carolina Platform High also known as the Cape Fear Arch (14-17). The structural features of this underlying basement rock influenced the extent of deposition and erosion of Cenozoic marine sediments that has occurred in response to numerous transgressive–regressive glacioeustactic sea-level cyclicity events over the course of approximately the last 18 million years (16-18). In particular, extensive deposition occurred in Onslow Bay during sea-level highstands associated with the Mid-Miocene Climatic Optimum, whereas extensive seafloor erosion and modification occurred in response to the Pleistocene Last Glacial Maximum and Holocene transgression (16, 19-24). As a result, sediments of the Miocene Pungo River and Pliocene Yorktown formations occur at or just below the seafloor across much of Onslow Bay and adjacent to the submerged ancestral Cape Fear River Valley.

The submerged Onslow Bay study localities previously described by Maisch *et al*. (23, 24) are the source of the Miocene and Pliocene megatoothed shark teeth and marine vertebrate fossils analyzed in this study. These localities occur on the gently sloping continental shelf of southwestern Onslow Bay at distances of approximately 30, 40, and 60 km from the present

shoreline, and at depths of approximately 25, 30, and 35 m, respectively. All submerged shelf localities consist of low-relief hardbottom scarps (<1,000 m^2) with adjacent lag deposits composed of well-rounded and poorly sorted, cobble, pebble, and sand-sized clasts that contain an abundance of megatoothed shark teeth. Larger clasts occurring in these lag deposits consist of sandstone, limestone, and quartz pebbles along with bioclasts including megatoothed shark teeth belonging to *Otodus megalodon* and *O. chubutensis* in addition to other Miocene and Pliocene shark teeth, marine mammal bones and teeth, and infrequent Pleistocene terrestrial mammal teeth (23, 24). Comparison of substrate and fossil samples to prior research on land-based and submerged Miocene-Pliocene exposures in North Carolina, identifies the limestone scarp and underlying brown-gray clay at the shallower shelf locality as the Pungo River Formation and the limestone scarp and underlying gray-blue clay present at the intermediate and deeper shelf localities as the Yorktown Formation (22-26). These identifications are also consistent with the stratigraphic and formation boundaries of substrate sediments in Onslow Bay constructed by Snyder *et al.* (14) and Snyder *et al*. (27, 28). For additional descriptions of the Pungo River and Yorktown formations from Onslow Bay can be found in Maisch *et al*. (23, 24).

At the shallower shelf locality, both *O. megalodon* and *O. chubutensis* teeth can be collected. In this regard, the *O. megalodon* teeth occurring along the surface of the Pungo River Formation represent bioclasts eroded from the overlying Yorktown Formation that was originally deposited at this locality. Only teeth belonging to *O. megalodon* and other distinctly Pliocene taxa from the Yorktown Formation are found at the intermediate and deeper shelf localities. At east of the submerged shelf localities, many of the vertebrate fossils exhibit variable degrees of taphonomic wear, carbonaceous encrustation, and bioerosion that attest to a complex taphonomic history associated with both glacioeustactically driven sea-level fluctuation and the effects of modern coastal storm events (23, 29, 30).

In reference to the present study, an abundance of elasmobranch teeth including those belonging to megatoothed sharks (*Otodus chubutensis*, *O. megalodon*, *Carcharodon hastalis, C. carcharias*, and *Parotodus benedini*), lamniforms (*Isurus oxyrinchus*), carcharhiniforms (*Carcharhinus* sp.), and marine mammal remains (i.e., inner ear bones of cetaceans) were recovered from the submerged Onslow Bay shelf localities. Taxa in the Onslow Bay assemblage are also known from land-based exposures along the Atlantic Coastal Plain of the United States (26, 31-33) and from contemporaneous shallow marine strata elsewhere around the world (34-44). The widespread geographic distribution of the Onslow Bay taxa attests to the uniformity of Miocene and Pliocene ocean conditions and migratory abilities of Late Cenozoic lamniform and

carcharhiniform sharks. The abundance and global distribution of many of the lamniform and carcharhiniform taxa found in Onslow Bay demonstrates the utility of these fossil teeth in regional and global biostratigraphic correlations. Moreover, these chondrichthyan teeth can also serve as geochemical proxies for interpreting ancestral ocean conditions and the thermophysiology of extinct taxa as is the focus of this study.

Additional samples of *C. hastalis* were analyzed from the Pliocene Duplin Formation of South Carolina. The Duplin Formation also contains marine invertebrates and vertebrates and has been regarded as a lateral equivalent to the Yorktown Formation (45, 46).

Specimens from Kuzubukuro, Higashi-matsuyama City, Saitama Prefecture, Japan

The fossil samples in this study representing the middle Miocene of Japan consist of a tooth of *Otodus megalodon* and an inner ear bone of a dolphin (Odontoceti) from the Godo Formation [(or the Godo Conglomerate Member of the Iwadono Formation (47)] at Kuzubukuro, Higashi-matsuyama City, Saitama Prefecture. The Godo Formation is composed of conglomerate and cross-bedded sandstone, and while its base is not observable, it is assumed to be at least 15 m thick and overlies the Ichinokawa Formation unconformably (48). Besides *O. megalodon* and cetacean fossils, known marine vertebrate from the Godo Formation include diverse sharks (e.g., *Dalatias licha*, *Pristiophorus* sp., *Carcharias cuspidate*, *Carcharodon hastalis*, *Isurus planus*, *I. desori*, *Parotodus benedini*, and *Carcharhinus* spp.) as well as desmostylians (Mammalia) (47, 49). The Godo Formation is considered to be Middle Miocene (Langhian) in age, about 15.1 Ma (48).

Specimens from Nagasaki-hana, Choshi City, Chiba Prefecture, Japan

The fossil samples in this study representing the early Pliocene of Japan include teeth of *Otodus megalodon, Carcharodon carcharias,* and *Carcharias* sp., that were collected from the Na-arai Formation at Nagasaki-hana in Choshi City, Chiba Prefecture. Besides the examined taxa, the Na-arai Formation is also known to yield other shark taxa, such as *Dalatias licha*, *Pristiophorus* sp., *Isurus oxyrinchus*, *Parotodus benedini*, *Hemipristis serra*, *Carcharhinus* spp., *Negaprion* sp., and *Sphyrna* sp. (50). The Na-arai Formation is represented by a marine conglomerate deposit, and microfossils suggest a minimum age of 4.36 Ma (51). Boessenecker *et al*. (52) considered the age of the Na-arai Formation to be 5.33-4.36 Ma.

Specimens from San Mateo Formation and Sharktooth Hill Bonebed, California, USA

Fossil specimens of *Otodus megalodon, Carcharodon carcharias*, and Odontoceti analyzed here from the US West Coast were collected from the upper gravel units of the San Mateo Formation which consists of a thin unit of unconsolidated sandstones and conglomerates that outcrop near Oceanside, San Diego County, California (53). Faunal remains from this upper unit, interpreted to represent the distal margin of a submarine fluvial delta system (54), have been dated as early Pliocene (Zanclean) in age based on vertebrate biochronology (54).

Fossil teeth of *Carcharhinus* sp*., Physogaleus* sp*., Isurus planus,* and *Carcharodon hastalis* measured here were collected in the middle Miocene aged (Langhian) units of the Sharktooth Hill Bonehead sequence within the middle Round Mountain Silt in Kern County, California (55). Magnetic stratigraphy of middle section of the Sharktooth Hill Bonebed (56) shows that the section correlates with Chron C5Br (16.0-15.2 Ma), and terrestrial mammals from the section indicate it is of Hemingfordian to middle Barstovian in age, consistent with the magnetic stratigraphy (57, 58). Further stratigraphic details of the fossil assemblage associated with the Sharktooth Hill Bonehead can be found in refs 55 and 59.

Specimens from Baden-Württemberg, Germany

The fossil specimens analyzed here, recently reported in McCormack *et al*. (60), were recovered from two neighboring sandpits, Walbertsweiler and Rengetsweiler, located within the Ottnangian of middle Burdigalian age between the cities Messkirch and Pfullendorf (Sigmaringen County). Marine fossil assemblages were deposited in this section of the Ottnangian following a marine transgression of the western Paratethys in a southwest direction. The transgression is characterized by a ~50 m thick layer of glauconitic sands of the Heidenlöcher Schichten (61). Above this layer resides the Kalkofen Formation, a 20-70 m thick unit consisting of glauconitic sands and marls in the lowermost part, and a sequence of marls showing only minor glauconitic sand fractions (lenses) in the uppermost part (62). Above the Kalkofen Formation resides the Baltringen Formation (63), which is composed of a conglomeratic sandstone with a coarse to medium granular texture, followed by a unit of fine to medium granular sands called the 'Baltringer Horizon', a shallow marine deposit (62-64) containing multiple macrofossils including both invertebrate (e.g., clam shells) and vertebrate (e.g., sharks and rays) fossils (65-67).

Presently, the Walbertsweiler site is a recultivated sandpit comprising a 1.6 m thick segment of the Kalkofen Formation that is accessible. The geological profile of the site shows an

interchanging sequence of little compacted marl and coarsely granular sands (65). Organic debris and bedding planes with ripple marks point to a coastal, inner neritic to shallow marine environment. The water depth is estimated to have been less than 50 m based on the frequency of shallow water foraminifers (62, 64). A small number of analyses (n=2) were also conducted on fossil elasmobranch teeth recovered from the neighboring Rengetsweiler site in the Baltringer Formation.

Specimens from Gozo, Republic of Malta

The samples used here were collected in 1988 from the surface of an upper Burdigalian age phosphorite layer (C2) located within the Globigerina Limestone Formation. A full list of fossils collected at this site and details of the geological formation can be found in Menesini (68) and Ward & Bonavia (69). To summarize, Malta and Gozo are part of the carbonate platform that extends from southeastern Sicily (Italy) to Tunisia and West-Lybia. This carbonate platform represents the foreland of the Apennine-Sicilian-Maghrebian belt (70).

2.2 Bioapatite phosphate oxygen isotope analysis

Enameloid samples were powdered with a slow speed Dremel dental drill equipped with a 300 µm diamond-tipped bit, then silver phosphate was precipitated following Mine *et al*. (71). Briefly, samples were weighed to ~1.0 mg and dissolved in 2.0M HNO_3 overnight. The following day, CaF_2 was precipitated with 2.9M HF and 2.0M NaOH and the resulting pellet was rinsed with an additional 0.1M NaF. The phosphate-containing supernatant was transferred to a new microcentrifuge tube for silver phosphate precipitation with an Ag-amine solution (1.09M NH_4OH and 0.37M $AgNO_3$). To optimize $AgPO_4$ precipitation and prevent isotopic fractionation, the pH window was adjusted with 2.0M HNO_3 to a target range of 5.5 to 7.5 and allowed to react for 10min. Silver phosphate crystals were centrifuged to pellet, rinsed five times with distilled water, then oven dried overnight at 50°C. In addition to samples, NIST 120C and a synthetic hydroxyapatite were prepared alongside as an additional prep standard.

The phosphate-oxygen stable isotopes ($\delta^{18}O_p$) were measured on a TCEA coupled with a Delta V Plus continuous flow IRMS with a Conflo IV at the Stable Isotope Ecosystem Laboratory of UC Merced (SIELO). All samples were weighed and analyzed in triplicate with individual subsample weighed to 0.15-0.20 mg in silver capsules. In some select cases, only duplicates

comprise the replicate if one run was >1.0‰ different from the other two runs; these samples are noted in the complete, archived data file on EarthChem.

The calibrated reference materials used were: USGS 80 (n=33, $\delta^{18}O = 13.3 \pm 0.4$‰); USGS 81a (n = 32, $\delta^{18}O = 35.5 \pm 0.4$‰); IAEA 601 (n =20, $\delta^{18}O = 23.0 \pm 0.7$‰). These reference materials allowed for linearity and drift corrections as well as normalization.

2.3 Bayesian Modeling

Bayesian models attempt to estimate the probable values of unknown parameters [in our case temperature and seawater $\delta^{18}O$ ($\delta^{18}O_{sw}$)] based on data ($\delta^{18}O_p$) and prior information about these parameters. This relationship is formalized in Bayes' theorem where:

$$P(T, \delta^{18}O_{sw} | \delta^{18}O_p) = \frac{P(\delta^{18}O_p | T, \delta^{18}O_{sw})}{P(\delta^{18}O_p)} \times P(T, \delta^{18}O_{sw})$$

The first term on the right-hand side of this equation is known as the *likelihood* and is the conditional probability of our data, given a proposed temperature and value of $\delta^{18}O_{sw}$. The second term represents our *prior* assumptions about these parameters. We defined the prior probabilities for the oxygen isotope composition and temperature of seawater as vague uniform distributions:

$$P(\delta^{18}O_{sw}) = U(min_{\delta 18O}, max_{\delta 18O})$$

$$P(T) = U(min_T, max_T)$$

Where the maximum and minimum values of $\delta^{18}O_{sw}$ span a plausible range of values considering: (1) modern gridded seawater values (72); and previous estimates from prior publications [e.g., Williams *et al*. (73) for the North Carolina specimens; *Dataset S1*]. The maximum and minimum seawater temperatures for each locality and time period were inferred from a recent 109-member ensemble of climate model simulations (HadCM3), which show strong model-proxy agreement for the global ocean for the Phanerozoic (74).

We defined the likelihood of our measured $\delta^{18}O_p$ values as:

$$\delta^{18}O_p \sim N(\mu, \sigma)$$

where μ is the equation of Kolodny *et al*. (75):

$$\mu = \delta^{18}O_{sw} - (temperature - 113.3) \div 4.38$$

and σ is a dispersion term estimated from the data. Combining these equations gives the final joint probability of:

$$P(T, \delta^{18}O_{sw} | \delta^{18}O_p) = N(\mu, \sigma) \times U(min_T, max_T) \times U(min_{\delta 18O}, max_{\delta 18O})$$

Table S1. Sea surface temperature and $\delta^{18}O_{sw}$ ranges used as prior information. See *Dataset S1* (as separate xlsx file) for locality specific temperature ranges.

Group	Temperature (°C)	$\delta^{18}O_{sw}$
Ectothermic	varied by locality	1 - 2
Regionally endothermic	10 - 40	1 - 2
Endothermic	10 - 45	1 - 2
Otodus megalodon/chubutensis	10 - 40	1 - 2
Carcharodon carcharias	10 - 40	1 - 2

We implemented our model in R (R Core Team, 2022) using an adaptive Markov Chain Monte Carlo Metropolis algorithm (76) with 50,000 iterations with 5,000 burn in to generate a representative posterior sample of $\delta^{18}O_{sw}$ and temperature for each fossil locality. We validated our approach using $\delta^{18}O_p$ values of teeth from two species of aquarium-reared (New York City Aquarium) shark species, *Carcharhinus plumbeus* and *Carcharias taurus*, where the water temperature is known (*Dataset S1*). We use a uniform prior of 10 – 40 °C for temperature and a gaussian prior of 0.0±1.0‰ (mean±2σ) for $\delta^{18}O_{sw}$ reflecting the range of oxygen isotope composition in a well-mixed modern ocean. Our model predicts a growth temperature of 20.7±6.2 °C (mean±2σ) which encompasses the true growth temperature of ~23 °C for these sharks. Our modeling code and full posterior sample for each group is available at github.com/robintrayler/bayesian_phosphate.

Table S2. Bayesian modeling posteriors for each locality. *Otodus* minus ectothermic-inferred ambient seawater temperatures (ΔT) were calculated separately for each location and time period.

Region	Thermoregulation or specific taxa	$\delta^{18}O_p$			$\delta^{18}O_{sw}$		Temperature (°C)		*Otodus* minus ectotherm temp. (ΔT)
		Mean	1s	n	Mean	1s	Mean	1s	
Global	ectotherm	22.1	0.7	28	1.5	0.3	21.3	1.4	
	endotherm	20.0	0.8	8	1.5	0.3	32.2	2.0	
	Regional endotherm	22.0	0.9	23	1.5	0.3	24.7	1.5	
	Otodus	21.3	0.6	16	1.5	0.3	27.0	2.0	
Miocene California	ectotherm	22.5	1.1	3	1.4	0.3	17.1	1.4	
	endotherm	19.8	0.3	3	1.5	0.3	32.9	3.2	
	Regional endotherm	21.7	0.6	2	1.5	0.3	25.5	4.6	
	Otodus megalodon	21.4	0.5	2	1.5	0.3	25.8	4.0	**8.7**
	Carcharodon carcharias	22.3	0.2	1	1.5	0.3	23.5	6.4	
Miocene Germany	ectotherm	22.5	1.1	12	1.5	0.3	21.2	1.6	
	Regional endotherm	21.8	0.4	2	1.5	0.3	23.9	4.5	
	Otodus chubutensis	20.5	0.4	2	1.5	0.3	29.7	3.6	**8.5**
Miocene Malta	ectotherm	21.9	0.7	5	1.5	0.3	22.9	2.1	
	Regional endotherm	21.5	0.5	1	1.5	0.3	25.2	6.0	
	Otodus chubutensis	21.1	0.6	2	1.5	0.3	27.0	3.9	**4.1**
Miocene Japan	endotherm	18.5	0.1	1	1.5	0.3	35.6	6.6	
	Otodus megalodon	21.6	0.2	1	1.5	0.3	25.1	5.7	
Pliocene Japan	ectotherm	22.9	0.3	2	1.5	0.3	19.7	4.1	
	Otodus megalodon	21.0	0.6	7	1.5	0.3	27.1	3.4	**7.4**
	Carcharodon carcharias	21.6	1.2	5	1.5	0.3	25.4	2.9	
Miocene North Carolina	Ectotherm	22.8	0.3	3	1.5	0.3	20.2	3.4	
	Endotherm	22.3	0.3	1	1.5	0.3	30.1	6.3	
	Regional endotherm	22.0	0.1	1	1.5	0.3	24.2	5.7	
	Otodus chubutensis	21.5	0.3	2	1.5	0.3	27.3	5.6	**7.1**
Pliocene North Carolina	Ectotherm	22.9	0.5	6	1.5	0.3	19.4	2.3	
	Endotherm	20.5	0.5	4	1.5	0.3	29.7	3.1	
	Regional endotherm	21.8	0.4	5	1.5	0.3	24.2	3.3	
	Otodus megalodon	21.5	0.6	6	1.5	0.3	26.1	3.1	**6.7**
	Carcharodon carcharias	23.0	1.0	7	1.5	0.3	19.1	2.6	
Average (1s)									**6.9 (1.6)**

3. Supplementary Discussion

3.1 Preservation of fossil bioapatite

The success of geochemical techniques requires that fossil bioapatite was not exposed to post burial diagenetic alteration via exchange with pore fluids and/or isotopic resetting due to bioapatite recrystallization, compaction and lithification. Hence, prior to making any inferences on the body temperatures of ancestral sharks from Δ_{47} and $\delta^{18}O_p$ in fossil shark teeth, we must rule out any potential for diagenetic alteration corrupting the geochemical compositions. In the case of fossil shark teeth, enameloid bioapatite is more likely to preserve the original isotopic composition compared with the inner dentine given the greater resistance to post depositional alteration from its dense microcrystalline structure (77, 78). While our conclusions are drawn from analyses conducted only on the enameloid phase of each tooth where diagenetic alteration has previously been ruled out from various other isotope work on these same samples (60, 79, 80), we nonetheless provide a suite of tests to establish the preservation potential of each specimen.

First, we conducted tandem Δ_{47} measurements on the dentine phase of each tooth using dentine as a benchmark against the enameloid for complete diagenetic alteration (*Dataset S2*). Results show significant (i.e., beyond analytical uncertainties) dentine-enameloid differences in Δ_{47}-derived temperatures between most tooth samples (Fig. S3). Average Δ_{47}-derived temperatures of North Carolina *Otodus megalodon* dentine are warmer than enameloid Δ_{47}-derived temperatures by 9 °C while *Carcharias carcharias* dentine from the same formation are warmer than enameloid derived temperatures by 3 °C. The South Carolina *C. hastalis* specimens, however, exhibit an opposite trend, wherein the dentine phase is 6 °C colder than the enameloid phase. Our *C. carcharias* specimens from Japan show a similar trend with the dentine phase yielding a Δ_{47}-derived temperature 10 °C colder than the enameloid phase. This apparent disparity in the temperature relationship between proposed diagenetic end-member materials could be explained by the presence of two different modes of diagenetic processes operating on the collected specimens. The warmer temperatures of the dentine phase relative to enameloid in North Carolina specimens could have resulted from late post-depositional recrystallization at elevated temperatures associated with burial. Conversely, colder temperatures exhibited by the dentine phase in specimens from Japan could be explained by early post depositional diagenetic alteration resulting from recrystallization under seafloor environmental conditions. Offsets suggesting a variable diagenetic influence on dentine and enameloid were also observed with $\delta^{13}C$ between the

two phases. Across all taxa and localities, dentine material yielded lower $\delta^{13}C$ values than enameloid from the same tooth.

Second, the Δ_{47} and $\delta^{18}O_p$ derived temperatures for fossil taxa are homogenous across five locations with distinct depositional environments and are within the range of what we would expect based on modern equivalent taxa (*Table S2* and *Dataset S1-S2*). The Bayesian $\delta^{18}O_p$ body temperature estimates of teeth from ectothermic shark taxa collected from the Pliocene strata of North Carolina (*Dataset S1*), which yield an average temperature of 19.2 ± 2 °C, also show excellent agreement with sea surface temperature estimates derived from Δ_{47} in scallops (21 ± 4 °C, n=13; *Chesapecten jeffersonius, Carolinapecten eboreus,* and *Placopecten clintonius*) from the same locality and time period. Moreover, prior oxygen isotope work on shells from the North Carolina site show sea surface temperatures that are consistent with the $\delta^{18}O_p$ body temperatures of our ectothermic sharks and Δ_{47} temperatures of the scallop shells (73). On the other hand, it is possible that at least partial alteration of the shells could have shifted the Δ_{47} temperatures in the scallops towards the higher diagenetic end-member indicated by the tooth dentine, which would preclude such a comparison between the enameloid and shells in the context of alteration. Nevertheless, the general agreement between the application of these two distinct proxies on two different substrate types (i.e., carbonate vs. phosphate) provides supporting evidence that the samples analyzed are likely free of diagenetic alteration and can be utilized to estimate environmental temperature conditions at these locations. What is more, it could be argued that the consistent differences amongst species across each locality (Fig. 1) would also suggest little or no alteration of the enameloid as complete alteration of all phosphate during diagenesis would tend to homogenize the values measured.

Previous work by our group utilizing enameloid-bound $\delta^{15}N$ (80) and $\delta^{66}Zn$ (60) isotopes to infer Cenozoic shifts in elasmobranch trophic levels from the same subset of specimens reported here showed remarkable homogeneity in both proxies through space and time (i.e., the Cenozoic). In both studies, extant elasmobranch species were also consistent with equivalent taxa in the fossil record, again arguing against alteration of the fossil specimens. Similar to our approach adopted here, where we find significant differences in Δ_{47} temperatures between the enameloid and dentine phases of the fossil teeth, McCormack *et al*. (60) also found significant differences in Zn isotopes between the two phases, interpreted to reflect alteration of the dentine while preservation of the enameloid.

In summary, while diagenetic alteration cannot be completely ruled out, these lines of evidence combined with our previous work suggests robust preservation of the fossil enameloid samples with minimal diagenetic alteration.

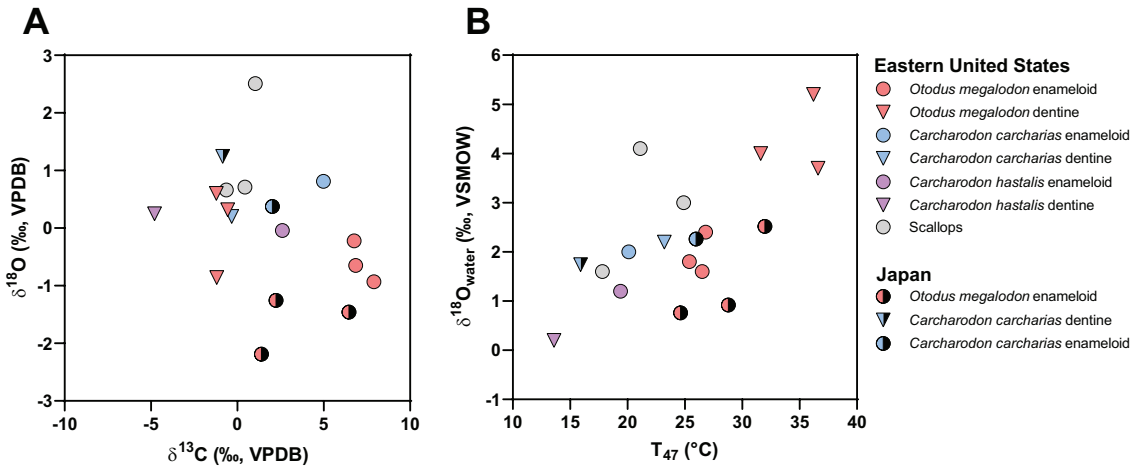

Fig. S3. (A, B) Comparison of enameloid and dentine materials. **(A)** comparison of water $\delta^{18}O$ and Δ_{47}-temperature estimates **(B)** between enameloid (circles) and dentine (triangles) shows that the coldest and warmest temperature estimates are represented by dentine material while enameloid plots in a comparably narrow region of temperature and water $\delta^{18}O$ which suggests that dentine samples, known to be more prone to diagenetic alteration than enameloid, may have undergone varying modes of post-depositional recrystallization.

4. Supplementary References

1. H. G. Ferrón, Regional endothermy as a trigger for gigantism in some extinct macropredatory sharks. *PLoS One* **12**, e0185185 (2017).
2. A. Bernard *et al.*, Regulation of body temperature by some Mesozoic marine reptiles. *Science* **328**, 1379-1382 (2010).
3. N. Anderson *et al.*, A unified clumped isotope thermometer calibration (0.5–1,100 C) using carbonate-based standardization. *Geophysical Research Letters* **48**, e2020GL092069 (2021).
4. N. Löffler *et al.*, Refining the temperature dependence of the oxygen and clumped isotopic compositions of structurally bound carbonate in apatite. *Geochimica et Cosmochimica Acta* **253**, 19-38 (2019).
5. S. V. Petersen *et al.*, Effects of improved ^{17}O correction on interlaboratory agreement in clumped isotope calibrations, estimates of mineral-specific offsets, and temperature dependence of acid digestion fractionation. *Geochemistry, Geophysics, Geosystems* **20**, 3495-3519 (2019).
6. W. F. Defliese, A. Tripati, Analytical effects on clumped isotope thermometry: Comparison of a common sample set analyzed using multiple instruments, types of standards, and standardization windows. *Rapid Communications in Mass Spectrometry* **34**, e8666 (2020).
7. S. M. Bernasconi *et al.*, InterCarb: A community effort to improve interlaboratory standardization of the carbonate clumped isotope thermometer using carbonate standards. *Geochemistry, Geophysics, Geosystems* **22**, e2020GC009588 (2021).
8. R. A. Eagle *et al.*, Body temperatures of modern and extinct vertebrates from 13C-18O bond abundances in bioapatite. *Proceedings of the National Academy of Sciences* **107**, 10377-10382 (2010).
9. D. A. Stolper, J. M. Eiler, The kinetics of solid-state isotope-exchange reactions for clumped isotopes: A study of inorganic calcites and apatites from natural and experimental samples. *American Journal of Science* **315**, 363-411 (2015).
10. D. A. Stolper, J. M. Eiler, Constraints on the formation and diagenesis of phosphorites using carbonate clumped isotopes. *Geochimica et Cosmochimica Acta* **181**, 238-259 (2016).
11. C. Román Palacios *et al.*, BayClump: Bayesian Calibration and Temperature Reconstructions for Clumped Isotope Thermometry.
12. W. A. Brand, S. S. Assonov, T. B. Coplen, Correction for the 17O interference in δ (13C) measurements when analyzing CO2 with stable isotope mass spectrometry (IUPAC Technical Report). *Pure and Applied Chemistry* **82**, 1719-1733 (2010).
13. C. M. John, D. Bowen, Community software for challenging isotope analysis: First applications of 'Easotope'to clumped isotopes. *Rapid Communications in Mass Spectrometry* **30**, 2285-2300 (2016).
14. S. W. Snyder, A. C. Hine, S. R. Riggs, Miocene seismic stratigraphy, structural framework, and sea-level cyclicity: North Carolina continental shelf. (1982).
15. S. R. Riggs, L. L. York, J. F. Wehmiller, S. W. Snyder, Depositional patterns resulting from high-frequency Quaternary sea-level fluctuations in northeastern North Carolina. (1992).
16. B. Horton *et al.*, Holocene sea-level changes along the North Carolina Coastline and their implications for glacial isostatic adjustment models. *Quaternary Science Reviews* **28**, 1725-1736 (2009).

17. M. S. Harris *et al.*, Continental shelf landscapes of the southeastern United States since the last interglacial. *Geomorphology* **203**, 6-24 (2013).
18. D. Soller. (United States Government Printing Office Washington, DC, 1988).
19. S. R. Riggs, W. J. Cleary, S. W. Snyder, Influence of inherited geologic framework on barrier shoreface morphology and dynamics. *Marine geology* **126**, 213-234 (1995).
20. S. R. Riggs, S. W. Snyder, A. C. Hine, D. L. Mearns, Hardbottom morphology and relationship to the geologic framework; Mid-Atlantic continental shelf. *Journal of Sedimentary Research* **66**, 830-846 (1996).
21. P. E. Renaud, S. R. Riggs, W. G. Ambrose Jr, K. Schmid, S. W. Snyder, Biological-geological interactions: storm effects on macroalgal communities mediated by sediment characteristics and distribution. *Continental Shelf Research* **17**, 37-56 (1997).
22. L. Ward, D. Bohaska, Synthesis of paleontological and stratigraphic investigations at the Lee Creek Mine, Aurora, NC (1958–2007). *Geology and Paleontology of the Lee Creek Mine, North Carolina, IV. Virginia Museum of Natural History Special Publication* **14**, 325-436 (2008).
23. H. M. Maisch IV, M. A. Becker, J. A. Chamberlain Jr, Lamniform and carcharhiniform sharks from the Pungo River and Yorktown formations (Miocene–Pliocene) of the submerged continental shelf, Onslow Bay, North Carolina, USA. *Copeia* **106**, 353-374 (2018).
24. H. M. Maisch IV, M. A. Becker, J. A. Chamberlain Jr, Macroborings in Otodus megalodon and Otodus chubutensis shark teeth from the submerged shelf of Onslow Bay, North Carolina, USA: implications for processes of lag deposit formation. *Ichnos* **27**, 122-141 (2020).
25. S. R. Riggs, D. W. Lewis, A. K. Scarborough, S. W. Snyder, Cyclic deposition of Neogene phosphorites in the Aurora area, North Carolina, and their possible relationship to global sea-level fluctuations. (1982).
26. R. W. Purdy *et al.*, The neogene sharks, rays, and bony fishes from Lee Creek Mine, Aurora, North Carolina. *Smithsonian Contributions to Paleobiology* **90**, 71-202 (2001).
27. S. W. Snyder, P. M. Mallette, S. W. Snyder, A. C. Hine, S. R. Riggs, Overview of seismic stratigraphy and lithofacies relationships in Pungo River Formation sediments of Onslow Bay, North Carolina Continental Shelf. (1988).
28. S. D. Snyder, G. W. Esch, Trematode community structure in the pulmonate snail Physa gyrina. *The Journal of parasitology*, 205-215 (1993).
29. S. R. Riggs, W. G. Ambrose, J. W. Cook, S. W. Snyder, S. W. Snyder, Sediment production on sediment-starved continental margins; the interrelationship between hardbottoms, sedimentological and benthic community processes, and storm dynamics. *Journal of Sedimentary Research* **68**, 155-168 (1998).
30. P. A. Wren, L. A. Leonard, Sediment transport on the mid-continental shelf in Onslow Bay, North Carolina during Hurricane Isabel. *Estuarine, Coastal and Shelf Science* **63**, 43-56 (2005).
31. H. Maisch IV, M. Becker, J. Chamberlain Jr, Chondrichthyans from a lag deposit between the Shark River Formation (Middle Eocene) and Kirkwood Formation (Early Miocene), Monmouth County, New Jersey. *Paludicola* **10**, 149-183 (2015).
32. A. K. Hastings, A. C. Dooley, Fossil-collecting from the middle Miocene Carmel Church Quarry marine ecosystem in Caroline County, Virginia. *Field Guides* **47**, 77-88 (2017).
33. B. Kent, The cartilaginous fishes (chimaeras, sharks, and rays) of Calvert Cliffs, Maryland, USA. *The Geology and Vertebrate Paleontology of Calvert Cliffs, Maryland, USA. Smithsonian Contributions to Paleobiology* **100**, 233-227 (2018).

34. R. W. Boessenecker, A new marine vertebrate assemblage from the late Neogene Purisima formation in Central California, Part I: fossil sharks, bony fish, birds, and implications for the age of the Purisma formation West of the San Gregorio Fault. *PalArch's Journal of Vertebrate Palaeontology* **8**, 01-30 (2011).
35. T. Reinecke, S. Louwye, U. Havekost, H. Moths, *The elasmobranch fauna of the late Burdigalian, Miocene, at Werder-Uesen, Lower Saxony, Germany, and its relationship with early Miocene faunas on the North Atlantic, Central Paratethys and Mediterranean*. (Palaeo Publishing and Library, 2011), vol. 20.
36. T. Bor, T. Reinecke, S. Verschueren, *Miocene Chondrichthyes from Winterswijk-Miste, the Netherlands*. (Palaeo Publishing and Library vzw, 2012).
37. H. Cappetta. (Gustav Fischer Verlag, Munich, Germany, 2012).
38. C. Pimiento *et al.*, Sharks and rays (Chondrichthyes, Elasmobranchii) from the late Miocene Gatun formation of Panama. *Journal of Paleontology* **87**, 755-774 (2013).
39. C. Pimiento *et al.*, Early Miocene chondrichthyans from the Culebra Formation, Panama: a window into marine vertebrate faunas before closure the Central American Seaway. *Journal of South American Earth Sciences* **42**, 159-170 (2013).
40. J. D. Carrillo-Briceno *et al.*, A new Late Miocene chondrichthyan assemblage from the Chagres Formation, Panama. *Journal of South American Earth Sciences* **60**, 56-70 (2015).
41. J. D. Carrillo-Briceño, T. Argyriou, V. Zapata, R. Kindlimann, C. Jaramillo, A new early Miocene (Aquitanian) elasmobranchii assemblage from the la Guajira Peninsula, Colombia. *Ameghiniana* **53**, 77-99 (2016).
42. J. D. Carrillo-Briceño *et al.*, An early Neogene elasmobranch fauna from the southern Caribbean (western Venezuela). *Palaeontologia Electronica*, 1-31 (2016).
43. J. F. Betancort-Lozano, A. Lomoschitz, J. Meco, Early Pliocene fishes (Chondrichthyes, Osteichthyes) from Gran Canaria and Fuerteventura (Canary Islands, Spain). *Estudios Geológicos*, (2016).
44. W. Landini *et al.*, The late Miocene elasmobranch assemblage from Cerro Colorado (Pisco Formation, Peru). *Journal of South American Earth Sciences* **73**, 168-190 (2017).
45. L. W. Ward, R. Bailey, J. Carter, J. Horton, V. Zullo, Pliocene and early Pleistocene stratigraphy, depositional history, and molluscan paleobiogeography of the Coastal Plain. *The Geology of the Carolinas: University of Tennessee Press, Knoxville, Tennessee*, 274-289 (1991).
46. J. Owens, Geology of the Cape Fear arch region, Florence 2° sheet and northern half of the Georgetown 2° sheet, North and South Carolina. *US Geol. Surv., Map*, 1-1948 (1989).
47. K. Shimada, N. Inuzuka, in *Transactions and proceedings of the Paleontological Society of Japan. New series*. (Palaeontological Society of Japan, 1994), vol. 1994, pp. 553-577.
48. Y. Kurihara, *Middle and Late Miocene marine Bivalvia from the northern Kanto region, central Japan*. (National Museum of Nature and Science, 2010).
49. K. Shimada. (Japan Home Teacher Center, Tokyo, 1987), pp. 354-357.
50. T. Uyeno, Y. Matsushima, Comparative study of teeth from Naganuma Formation of Middle Pleistocene and Recent specimens of the great white shark, Carcharodon carcharias from Japan. *Bulletin of Kanagawa Prefectural Museum* **11**, 11-30 (1979).
51. T. Uyeno, Y. Kondo, K. Inoue, A nearly complete tooth set and several vertebrae of the lamnid shark Isurus hastalis from the Pliocene of Chiba, Japan. *Journal of the Natural History Museum and Institute, Chiba* **3**, 15-20 (1990).
52. R. W. Boessenecker *et al.*, The Early Pliocene extinction of the mega-toothed shark Otodus megalodon: a view from the eastern North Pacific. *PeerJ* **7**, e6088 (2019).

53. L. Barnes, H. Howard, J. Hutchison, B. Welton, P. Abbott, The vertebrate fossils of the marine Cenozoic San Mateo Formation at Oceanside, California. *Geologic investigations of the coastal plain San Diego County, California*, 53-70 (1981).
54. D. P. Domning, T. A. Deméré, New material of Hydrodamalis cuestae (Mammalia: Dugongidae) from the Miocene and Pliocene of San Diego County, California. *Transactions of the San Diego Society of Natural History* **20**, 169-188 (1984).
55. H. C. Olson, Oligocene-middle Miocene depositional systems north of Bakersfield, California: eastern basin equivalents of the Temblor Formation (1988).
56. D. R. Prothero, F. Sanchez, L. L. Denke, Magnetic stratigraphy of the Early to Middle Miocene Olcese Sand and Round Mountain Silt, Kern County, California. *New Mexico Museum of Natural History and Science Bulletin* **44**, 357-363 (2008).
57. M. Liter, D. Prothero, J. O'Connor, Land Mammals from the Middle Miocene Round Mountain Silt, Northeast of Bakersfield, California. *Bakersfield, California: Pacific Section American Association of Petroleum Geologists, Society of Economic Paleontologists and Mineralogists, and Society of Exploration Geophysicists*, 9-12 (2004).
58. D. R. Prothero *et al.*, Land mammals from the Middle Miocene Sharktooth Hill Bonebed, Kern County, California. *New Mexico Museum of Natural History and Science Bulletin* **44**, 299-314 (2008).
59. B. J. Welton, A new fossil basking shark (Lamniformes: Cetorhinidae) from the middle Miocene Sharktooth Hill bonebed, Kern County, California. *Contributions in Science* **522**, 29-44 (2014).
60. J. McCormack *et al.*, Trophic position of Otodus megalodon and great white sharks through time revealed by zinc isotopes. *Nature Communications* **13**, 2980 (2022).
61. G. Doppler, K. Heissig, B. Reichenbacher, Die Gliederung des Tertiärs im süddeutschen Molassebecken. *Newsletters on Stratigraphy*, 359-375 (2006).
62. N. Heckeberg, M. Pippèrr, B. Läuchli, F. U. Heimann, B. Reichenbacher, The Upper Marine Molasse (Burdigalian, Ottnangian) in Southwest Germany-facies interpretation and a new lithostratigraphic terminology. *Zeitschrift der Deutschen Gesellschaft fur Geowissenschaften* **161**, 285 (2010).
63. F. U. Heimann, D. U. Schmid, M. Pipperr, B. Reichenbacher, Re-interpreting the Baltringer Horizont as a subtidal channel facies: Implications for a new understanding of the Upper Marine Molasse" Cycles"(Early Miocene). *Neues Jahrbuch Fur Geologie Und Palaontologie-Abhandlungen* **254**, 135 (2009).
64. M. Pippèrr, Characterisation of Ottnangian (middle Burdigalian) palaeoenvironments in the North Alpine Foreland Basin using benthic foraminifera—a review of the Upper Marine Molasse of southern Germany. *Marine Micropaleontology* **79**, 80-99 (2011).
65. D. Barthelt, Notizen zu einem Profil der Selachier-Fundstelle Walbertsweiler im Bereich der Miozan Oberen meeresmolasse Suddeutchlands. *Munchener Geowiss Abh (A)* **19**, 195-208 (1991).
66. J. Probst, Beitrage zur Kenntniss der fossilen Fische aus der molasse von Baltringen. II: Batoïdei A. *Günther. Jahresh. Ver. Naturk. Württemberg* **33**, 69-103 (1877).
67. J. Probst, Beiträge zur Kenntniss der fossilen Fische aus der Molasse von Baltringen. . *Günther. Jahresh. Ver. Naturk. Württemberg* **35**, 127-191 (1879).
68. E. Menesini, Ittiodontoliti delle formazioni terziaire dell' arcipelago maltese. *Palaeontographia Italica* **67**, 121-161 (1974).
69. D. J. Ward, C. Galea Bonavia, Additions to, and a review of, the Miocene shark and ray fauna of Malta. (2001).

70. M. Martinelli, A. Bistacchi, F. Balsamo, M. Meda, Late Oligocene to Pliocene extension in the Maltese Islands and implications for geodynamics of the Pantelleria Rift and Pelagian Platform. *Tectonics* **38**, 3394-3415 (2019).
71. A. Mine *et al.*, Microprecipitation and $\delta^{18}O$ analysis of phosphate for paleoclimate and biogeochemistry research. *Chemical Geology* **460**, 1-14 (2017).
72. A. N. LeGrande, G. A. Schmidt, Global gridded data set of the oxygen isotopic composition in seawater. *Geophysical research letters* **33**, (2006).
73. M. Williams *et al.*, Pliocene climate and seasonality in North Atlantic shelf seas. *Philosophical Transactions of the Royal Society A: Mathematical, Physical and Engineering Sciences* **367**, 85-108 (2009).
74. P. J. Valdes, C. R. Scotese, D. J. Lunt, Deep ocean temperatures through time. *Climate of the Past* **17**, 1483-1506 (2021).
75. Y. Kolodny, B. Luz, O. Navon, Oxygen isotope variations in phosphate of biogenic apatites, I. Fish bone apatite—rechecking the rules of the game. *Earth and Planetary Science Letters* **64**, 398-404 (1983).
76. H. Haario, E. Saksman, J. Tamminen, An adaptive Metropolis algorithm. *Bernoulli*, 223-242 (2001).
77. P. L. Koch, R. Michener, K. Lajtha, Isotopic study of the biology of modern and fossil vertebrates. *Stable isotopes in ecology and environmental science* **2**, 99-154 (2007).
78. A. Zazzo, C. Lécuyer, S. M. Sheppard, P. Grandjean, A. Mariotti, Diagenesis and the reconstruction of paleoenvironments: a method to restore original $\delta^{18}O$ values of carbonate and phosphate from fossil tooth enamel. *Geochimica et Cosmochimica Acta* **68**, 2245-2258 (2004).
79. A. A. Akhtar *et al.*, A record of the $\delta^{44/40}Ca$ and [Sr] of seawater over the last 100 million years from fossil elasmobranch tooth enamel. *Earth and Planetary Science Letters* **543**, (2020).
80. E. R. Kast *et al.*, Cenozoic megatooth sharks occupied extremely high trophic positions. *Science Advances* **8**, eabl6529 (2022).